Angular dependence of dissociative electron attachment to polyatomic molecules: Application to the $^2B_1$ metastable state of the H_2O and H_2S anions

Daniel J. Haxton,[1,2,*] C. William McCurdy,[2,3,†] and Thomas N. Rescigno[2,‡]
[1]*Department of Chemistry, University of California, Berkeley, California 94720, USA*
[2]*Lawrence Berkeley National Laboratory, Chemical Sciences, Berkeley, California 94720, USA*
[3]*Departments of Applied Science and Chemistry, University of California, Davis, California 95616, USA*
(Received 1 March 2006; published 30 June 2006)

The angular dependence of dissociative electron attachment (DEA) to polyatomic targets is formulated in the local complex potential model, under the assumption that the axial recoil approximation describes the dissociation dynamics. An additional approximation, which is found to be valid in the case of H_2O but not in the case of H_2S, makes it possible to describe the angular dependence of DEA solely from an analysis of the fixed-nuclei entrance amplitude, without carrying out nuclear dynamics calculations. For H_2S, the final-vibrational-state-specific angular dependence of DEA is obtained by incorporating the variation of the angular dependence of the entrance amplitude with nuclear geometry into the nuclear dynamics. Scattering calculations using the complex Kohn method and, for H_2S, full quantum calculations of the nuclear dynamics using the multiconfiguration time-dependent Hartree method, are performed.

DOI: 10.1103/PhysRevA.73.062724 PACS number(s): 34.80.Ht

I. INTRODUCTION

The *ab initio* computation of the cross section for dissociative electron attachment (DEA) to H_2O has been addressed in two previous works [1,2]. Both H_2O [3–16] and H_2S [17] undergo dissociative attachment via several metastable states of the anion. In particular, both molecules have a Feshbach resonance of $^2B_1$ symmetry which participates in this process. In our previous work on H_2O, we calculated the cross sections for DEA via this resonance state using complex Kohn scattering calculations [18,19] and quantum nuclear dynamics calculations employing the multiconfiguration time-dependent Hartree (MCTDH) method [20–23], and succeeded in closely reproducing experimentally determined quantities such as the total cross section and degree of vibrational excitation of the OH fragment. The present paper is concerned with the calculation of angular dependences for the production of H^- ions from the $^2B_1$ resonance state of either anion, i.e.,

$$H_2O + e^- \rightarrow H_2O^-(^2B_1) \rightarrow H^- + OH\ (X\ ^2\Pi), \qquad (1a)$$

$$H_2S + e^- \rightarrow H_2S^-(^2B_1) \rightarrow H^- + SH\ (X\ ^2\Pi). \qquad (1b)$$

To be precise, what is meant by "angular dependence" is the dependence of the cross section on the H^- scattering angle θ, which is defined by the schematic in Fig. 1. This is the angle between the direction of the incident beam of electrons and that of the ejected H^- ions produced in the experiment.

The experimental results on DEA to these molecules via the $^2B_1$ resonance state indicate that in the H_2O case the angular dependence of the cross section for different final vibrational states of OH is relatively similar [9,10]. In contrast, for DEA to H_2S, there is a significantly different angular dependence for production of the ground and first excited vibrational state of SH [17]. At high incident electron energies, the second vibrational state is observed in greater proportion to the first at θ=45°, but in lesser proportions at greater angles.

The calculations presented here reproduce this effect, which arises from a combination of two factors. The first is the mixing of different partial waves into the "entrance amplitude" for production of the resonant state. The entrance amplitude for dissociative attachment is analagous to the dipole matrix element which controls the amplitude for photodissociation. The entrance amplitude depends upon the initial orientation of the molecule with respect to the incident electron beam and this dependence leads to an angular dependence in the cross section, even after it is averaged over the random orientations of the molecule with respect to the incident electron direction. In H_2S, the dependence of the entrance amplitude on molecular orientation changes appreciably as the *internal* nuclear geometry varies within the Franck-Condon region, whereas for H_2O, it does not. As a result, the nuclear dynamics for the dissociation of H_2S^- $(^2B_1)$ are different depending on the original orientation of the H_2S molecule relative to the incident electron beam at the time of attachment.

The second factor is the "axial recoil" [24] nature of the dissociation. The axial recoil approximation states that the recoil axis which connects the atom and the diatom center of

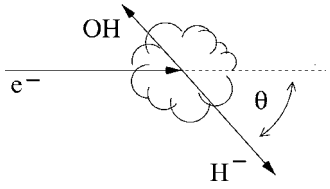

FIG. 1. Definition of H^- scattering angle θ.

*Electronic address: djhaxton@lbl.gov
†Electronic address: cwmccurdy@lbl.gov
‡Electronic address: tnrescigno@lbl.gov

mass does not rotate during the dissociation. If this is the case, then the probability for producing dissociative fragments at a certain orientation is the same as the probability for attachment at that orientation (if the survival probability for the dissociative species is unity). If the approximation does not apply, then the dependence of the entrance amplitude upon the initial orientation of the molecule will effectively be spread over a range of final orientations, and final-state-specific angular dependences are much less likely.

For each of these $^2B_1$ resonance states, that of H_2O and that of H_2S, the corresponding adiabatic potential energy surface is steeply dissociative but relatively flat with bend, near the equilibrium geometry of the neutral. Therefore, the axial recoil approximation may be applied, which simplifies the calculations considerably. The angular dependence of the DEA cross section to H_2O is found by simply evaluating the probability for electron attachment at each orientation θ, whereas for H_2S, we perform a separate nuclear dynamics calculation at each orientation.

The outline of this paper is as follows. In Sec. II, we describe the local complex potential (LCP), which introduces concepts such as the entrance amplitude which are necessary for understanding the DEA process. In Sec. III we introduce expressions for the dissociative attachment T-matrices. In Sec. IV we describe the axial recoil approximation, leaving a detailed derivation of this approximation for the Appendix. In Sec. V we describe our method for fitting the S-matrices obtained from scattering calculations to obtain partial wave amplitudes. In Sec. VI we present results for H_2O, and in Sec. VII we present results for H_2S. We conclude with a brief summary.

II. LOCAL COMPLEX POTENTIAL MODEL

For resonances such as the $^2B_1$ state of H_2O^- or H_2S^-, the dissociative attachment process may be treated under the local complex potential (LCP) model [24–28], which describes the nuclear dynamics of the resonant state in terms of the driven Schrödinger equation,

$$(E - H_a)\xi_{\nu_i}(\vec{Q}) = \phi_{\nu_i}(\vec{Q}), \tag{2}$$

in which H_a is the Hamiltonian for the nuclear motion of the resonant state,

$$H_a = T_{\vec{Q}} + E_R(\vec{q}_{\rm int}) - \frac{i\Gamma(\vec{q}_{\rm int})}{2}. \tag{3}$$

The nuclear degrees of freedom in the center-of-mass system are collectively denoted by $\vec{Q}$; the nuclear kinetic energy, by $T_{\vec{Q}}$. The electronic energy of the resonance is $E_R - i\Gamma/2$, where Γ is its width, and E_R is the real part of its energy. These quantities are functions of $\vec{q}_{\rm int}$, the internal degrees of freedom of the molecule, which are a subset of $\vec{Q}$. The resonance energy has a negative imaginary component, which leads to its decay.

As described elsewhere [29–31], Eq. (2) can be arrived at via the formalism of Feshbach [32] partitioning, in which the electronic Hilbert space of the molecular system is divided into resonant and nonresonant parts after the Born-Oppenheimer approximation is made. The resonant part of the Hilbert space (also called "Q-space") is the single discrete resonance state ψ_Q; the remainder of the Hilbert space is called "P-space," the members of which are denoted by ψ_P.

The driving term, ϕ_{ν_i} in Eq. (2), is defined as

$$\phi_{\nu_i}(\vec{Q}) = V_{\bar{a}}(\vec{Q})\chi_{\nu_i}(\vec{Q}), \tag{4}$$

in which χ_{ν_i} is the initial rovibrational wave function of the neutral target with quantum numbers ν_i, and the quantity $V_{\bar{a}}$ is the "entrance amplitude," defined as

$$V_{\bar{a}}(\vec{Q}) = [\psi_P(\vec{Q})|H_{\rm el}|\psi_Q(\vec{q}_{\rm int})], \tag{5}$$

where the brackets denote integration over the electronic degrees of freedom $\vec{r}_e$ (which are defined with respect to the body-fixed frame). The wave function ψ_P in the above matrix element is the nonresonant part of the electron scattering wave function, and therefore incorporates the boundary conditions which define the dissociative attachment problem, i.e., the energy and angular dependence of the incident electron wave function and the initial electronic state of the target. The entrance amplitude $V_{\bar{a}}$ is therefore dependent upon not only the internal degrees of freedom of the molecule, which affect the electronic wave function and electronic Hamiltonian of the initial and resonant state, but also upon the orientation of the molecule relative to the incident plane wave.

The latter dependence is often neglected, as it usually does not affect the calculated total cross sections, by using Fermi's golden rule to replace the entrance amplitude with an averaged quantity:

$$V_{\bar{a}}(\vec{Q}) \to \sqrt{\int d\bar{\Omega}|V_{\bar{a}}(\vec{Q})|^2} = \sqrt{\frac{\Gamma(\vec{q}_{\rm int})}{2\pi}}. \tag{6}$$

The integration in Eq. (6) is over the angular variables that orient the target in the laboratory frame, i.e., $\vec{Q}$ less the internal variables $\vec{q}_{\rm int}$. This approximation neglects the rotational excitation caused by the angular dependence of the entrance amplitude, and destroys all information about the angular dependence of the products.

The LCP equation, Eq. (2), may be formally inverted,

$$\xi_{\nu_i} = \hat{G}^+(E)\phi_{\nu_i}, \tag{7}$$

where $\hat{G}^+$ is the resolvent operator,

$$\hat{G}^+ = (E - H_a + i\epsilon)^{-1}. \tag{8}$$

The coordinate space representation of the resolvent is the outgoing wave Green's function G^+ and we have

$$\xi_{\nu_i}(\vec{Q}) = \int d\vec{Q}' G^+(\vec{Q};\vec{Q}';E)\phi_{\nu_i}(\vec{Q}'). \tag{9}$$

In practice, we represent the Green's function as the Fourier transform of the propagator, and thereby obtain the solution of Eq. (2) as

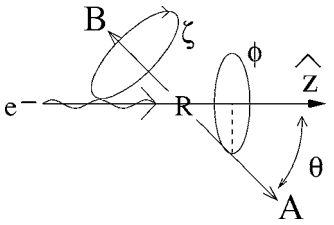

FIG. 2. Schematic of Euler angles ϕ, θ, ζ and dissociative coordinate R for general dissociative attachment problem. "A" and "B" stand for one or more atomic fragments of molecule AB and R is the distance between their centers of mass. A is the anion.

$$\xi_{\nu_i}(\vec{Q}) = \lim_{\epsilon \to 0} i \int_0^\infty e^{i(E+i\epsilon)t} e^{-iH_{a^t}} \phi_{\nu_i}(\vec{Q},0) dt$$

$$= \lim_{\epsilon \to 0} i \int_0^\infty e^{i(E+i\epsilon)t} \phi_{\nu_i}(\vec{Q},t) dt, \quad (10)$$

where we define the time-dependent nuclear wave function as

$$\phi_{\nu_i}(\vec{Q},t) = e^{-iH_{a^t}} \phi_{\nu_i}(\vec{Q},0). \quad (11)$$

We employ the MCTDH package [33] for the propagation of the driving term ϕ_{ν_i} and the subsequent analysis. Further details can be found in Ref. [2].

III. T-MATRICES FOR DISSOCIATIVE ATTACHMENT

For the moment, we will follow O'Malley [28] and not restrict our formalism to a triatomic or diatomic molecule. Considering a general dissociative attachment process

$$e^- + AB \to A^- + B, \quad (12)$$

where A and B may stand for one or more atomic components of the molecule AB, we define the dissociative coordinates as follows. The distance between the center of mass of A and the center of mass of B is called R. The orientation of the corresponding vector $\vec{R}$ (defined as pointing toward the anion A^-) is denoted by the angles θ and ϕ, defined relative to the laboratory-frame z axis and xz plane. We may refer to θ and ϕ collectively as the solid angle Ω_k. In a scattering problem it is useful to define the z axis as parallel to the wave vector of the incident electron. For a triatomic or greater, we may also specify ζ, the third Euler angle, which orients the molecule around the $\hat{R}$ axis. This setup is generally called an "R-embedding" coordinate system [34] and is summarized in Fig. 2.

Given a scattering wave function Ψ with incoming part normalized as

$$\Psi \underset{r_e \to \infty}{\sim} \sqrt{\frac{k}{2\pi^2}} e^{i\vec{k}\cdot\vec{r}_e} \Psi_{AB} + \text{outgoing components}, \quad (13)$$

the T-matrix for dissociative attachment is defined as the coefficient of the outgoing spherical wave [28],

$$\Psi \underset{R \to \infty}{\sim} \sum_{\tau\upsilon} T^{\tau\upsilon}_{\mathrm{DEA}}(\theta,\phi) \sqrt{\frac{\mu_R}{2\kappa_{\tau\upsilon}}} \frac{e^{i\kappa_{\tau\upsilon}R}}{R} (\Psi^\tau_{A^-} \times \Psi^\upsilon_B). \quad (14)$$

In these equations Ψ_{AB} is the full wave function (electronic and rovibrational) of the neutral target state, $\vec{k}$ is the wave vector of the incident electron, and $\vec{r}_e$ are its coordinates in the center-of-mass frame. Also, Ψ_{A^-} and Ψ_B are the full wave functions of the fragments A^- and B with rovibrational quantum numbers denoted collectively by τ and υ, and energies E_τ and E_υ, respectively; μ_R is the reduced mass in the dissociative coordinate R; and $\kappa_{\tau\upsilon}$ is the wave number of the recoil in that coordinate,

$$\kappa_{\tau\upsilon} = \sqrt{2\mu_R(E - E_\tau - E_\upsilon)}. \quad (15)$$

We may make the Born-Oppenheimer approximation for the initial and final states, and thereby define

$$\Psi^\tau_{A^-} = \psi^\tau_{A^-} \times \phi_{A^-},$$

$$\Psi^\upsilon_B = \psi^\upsilon_B \times \phi_B, \quad (16)$$

where the ψ are the rovibronic wave functions, and ϕ the electronic wave functions, of the final states, the latter of which depend parametrically upon the nuclear coordinates.

In terms of the driving term ϕ_{ν_i} of the LCP model we thereby obtain

$$T^{\tau\upsilon}_{\mathrm{DEA}}(\theta,\phi) = \lim_{R \to \infty} \sqrt{\frac{2\kappa_{\tau\upsilon}}{\mu_R}} \mathrm{Re}^{-i\kappa_{\tau\upsilon}R} (\psi^\tau_{A^-} \psi^\upsilon_B | G^+ | \phi_{\nu_i}) \quad (17)$$

in which the parenthetical notation $(|)$ denotes integration over all degrees of freedom except R and the solid angle Ω_k.

With the definition of the T-matrix from Eqs. (13) and (14), the definition of the differential cross section becomes [24]

$$\frac{\partial \sigma_{\mathrm{DEA}}}{\partial \Omega_k} = \frac{\pi}{k^2} |T_{\mathrm{DEA}}(\Omega_k)|^2 \quad (18)$$

such that

$$\frac{\partial \sigma^{\tau\upsilon}_{\mathrm{DEA}}}{\partial \Omega_k} = \lim_{R \to \infty} \frac{2\kappa_{\tau\upsilon}\pi}{\mu_R k^2} R^2 |(\psi^\tau_{A^-} \psi^\upsilon_B | G^+ | \phi_{\nu_i})|^2. \quad (19)$$

IV. AXIAL RECOIL APPROXIMATION

The axial recoil approximation [24] states that the orientation of the molecule in terms of the coordinates θ and ϕ does not change as the dissociation occurs. If this is the case, then the dependence upon orientation of the entrance amplitude is preserved in the angular dependence of the products. The applicability of this approximation is dependent upon the rotational temperature of the molecules dissociated in the experiment: if the sample is hot enough so that the rotational energy is comparable to the dissociation energy of the transient species involved, then the rotation of the dissociation axis during the dissociation is unavoidable; the axial recoil approximation does not apply, and the dissociative attachment cross section is likely to be isotropic.

From a practical standpoint, the axial recoil approximation helps to reduce the number of degrees of freedom which must be explicitly included in the numerical solution of Eq. (7).

For a diatomic, the axial recoil approximation requires only that the interatomic potential be steeply dissociative in R. For a polyatomic, this approximation is more stringent: not only must the potential be steeply dissociative so that the molecule rotates negligibly during the dissociation process, but in addition, there must not be internal dynamics which lead to the rotation of the dissociation axis $\hat{R}$ relative to the direction of the incident electron. For a triatomic, this means that the potential must be relatively flat in the Jacobi coordinate γ, which for H_2O and H_2S is almost equivalent to the bond angle θ_{HOH} or θ_{HSH}. We have found that the portions of the potential energy surfaces of both $^2B_1$ states which are sampled by the dissociating wave packets are indeed relatively flat in γ.

The axial recoil approximation requires there to be a Dirac delta function in the Green's function:

$$G^+(\vec{Q};\vec{Q}';E)\times\phi_{\nu_i}(\vec{Q}')=g^+(\vec{q};\vec{q}';E)\delta(\Omega_k-\Omega_k')\times\phi_{\nu_i}(\vec{Q}'), \tag{20}$$

in which expansion $\vec{q}$ stands for all coordinates contained in $\vec{Q}$ except for θ and ϕ. In the Appendix we provide a standard derivation of this approximation for a diatomic, and one for polyatomic targets as well.

For certain cases, the axial recoil approximation provides a means to derive a simple expression for the DEA angular dependence, which does require nuclear dynamics calculations for its evaluation. In those cases, in addition to the axial recoil approximation, an assumption about the entrance amplitude $V_{\bar{a}}$, which we will term the "constant-eigenmode approximation" for reasons that will be made clear below, needs to be made as well. The entrance amplitude may be expanded in a complete orthonormal angular basis y_μ, such that

$$V_{\bar{a}}(\vec{Q})=\sum_{\mu=1}^{\infty}V_\mu(\vec{q_{\rm int}})y_\mu(\bar{\Omega}), \tag{21}$$

where $\bar{\Omega}$ is either the angle θ for a diatomic or the solid angle $\{\theta,\zeta\}$ for a polyatomic, and

$$\int d\bar{\Omega}y_\nu^*(\bar{\Omega})y_\mu(\bar{\Omega})=\delta_{\nu\mu}. \tag{22}$$

(The entrance amplitude $V_{\bar{a}}$ does not depend on ϕ because of the symmetry of the incoming plane wave.)

We consider first the case of a diatomic target, for which the internal coordinate $\vec{q_{\rm int}}$ is R, the internuclear distance, and the initial rovibrational target state can be written as

$$\chi_{\nu_i}(\vec{Q})=\chi_{j_i\nu_i}(R)Y_{j_im_i}(\theta,\phi). \tag{23}$$

If only one member of the set $\{y_\mu\}$, say y_{μ_0}, contributes to the sum in Eq. (21), i.e.,

$$V_{\bar{a}}(\vec{Q})=V_{\mu_0}(\vec{q_{\rm int}})y_{\mu_0}(\bar{\Omega})=V_{\mu_0}(R)y_{\mu_0}(\theta), \tag{24}$$

then the driving term in Eq. (2) is factorable into an R-dependent part and a Ω_k-dependent part,

$$\phi_{\nu_i}(\vec{Q})=y_{\mu_0}(\theta)Y_{j_im_i}(\theta,\phi)[V_{\mu_0}(R)\chi_{j_i\nu_i}(R)]. \tag{25}$$

Equation (24) is the constant-eigenmode approximation. If the axial recoil approximation, Eq. (20), applies, then the differential cross section, Eq. (19), may then also be factored,

$$\frac{\partial\sigma_{\rm DEA}}{\partial\Omega_k}=\lim_{R\to\infty}\frac{2\kappa\pi}{\mu_R k^2}R^2|y_{\mu_0}(\theta)|^2|Y_{j_im_i}(\theta,\phi)|^2\times\left|\int dR'g^+(R;R';E)V_{\mu_0}(R)\chi_{j_i\nu_i}(R)\right|^2. \tag{26}$$

For a diatomic, an average over degenerate initial states is accomplished by averaging over the m_i quantum number; the $|Y_{j_im_i}(\theta,\phi)|^2$ terms in Eq. (26) average to $1/4\pi$ when this is done, and the cross section becomes proportional to $|y_{\mu_0}(\theta)|^2$. Thus, we obtain the angular dependence of the dissociative attachment products simply by evaluating the angular dependence of the entrance amplitude. We emphasize that this constant-eigenmode approximation does not mean that the cross section need be dominated by a single partial wave, since the angular function $y_{\mu_0}(\theta)$ may contain contributions from different l values. The only requirement is that the factorization implied by Eq. (24) hold over the Franck-Condon region of the initial target state.

For a polyatomic molecule, approximations beyond the axial recoil approximation of Eq. (20) and the constant-eigenmode approximation of Eq. (24) are necessary to derive this result, or more precisely, the result that

$$\frac{\partial\sigma_{\rm DEA}}{\partial\Omega_k}\propto\int d\zeta|y_{\mu_0}(\theta,\zeta)|^2 \tag{27}$$

after summing over inital and final rotational states. These are described in the Appendix.

Finally, if the constant-eigenmode approximation cannot be made, i.e., the entrance amplitude $V_{\bar{a}}$ within the Franck-Condon region cannot be factored into an $\bar{\Omega}$-dependent part and a $\vec{q_{\rm int}}$-dependent part as per Eq. (24), then we have

$$\frac{\partial\sigma_{\rm DEA}}{\partial\Omega_k}=\lim_{R\to\infty}\frac{2\kappa\pi}{\mu_R k^2}R^2|Y_{j_im_i}(\theta,\phi)|^2\times\left|\int dR'g^+(R;R';E)V_{\bar{a}}(R,\theta)\chi_{j_i\nu_i}(R)\right|^2, \tag{28}$$

and we may calculate final-state-specific cross sections by evaluating the dR' integral for different values of θ. In subsequent sections, we will develop an analagous expression for a polyatomic case and use it for calculations on H_2S.

V. CALCULATION OF $V_{\bar{a}}$

To obtain the angular dependence of the entrance amplitude $V_{\bar{a}}$, we begin with a result of formal scattering theory

which states that, in the vicinity of a narrow resonance, the T operator can be partitioned into resonant and nonresonant components

$$T(E) = T^{\mathrm{bg}} + T^{\mathrm{res}}(E), \tag{29}$$

where

$$T^{\mathrm{res}}(E) = -\pi \frac{V|\Psi^{\mathrm{res}}\rangle\langle\tilde{\Psi}^{\mathrm{res}}|V}{(E - E_{\mathrm{res}} + i\Gamma/2)}, \tag{30}$$

and that the (electronically elastic) resonance scattering amplitude, which is proportional to a matrix element of T^{res} on the energy shell, is thus

$$f^{\mathrm{res}}_{\vec{k}\to\vec{k}'} = \frac{1}{k}\langle\vec{k}'\Psi_o|T^{\mathrm{res}}|\vec{k}\Psi_o\rangle = -\frac{\pi}{k}\frac{\langle\vec{k}'\Psi_o|V|\Psi^{\mathrm{res}}\rangle\langle\tilde{\Psi}^{\mathrm{res}}|V|\vec{k}\Psi_o\rangle}{(E - E_{\mathrm{res}} + i\Gamma/2)}, \tag{31}$$

where k is the magnitude of both $\vec{k}$ and $\vec{k}'$; Ψ_o is the target wave function; and $\langle\vec{r_e}|\vec{k}\rangle$ is an energy normalized plane wave,

$$\langle\vec{r_e}|\vec{k}\rangle = \sqrt{k}\frac{1}{(2\pi)^{3/2}}e^{i\vec{k}\cdot\vec{r_e}}. \tag{32}$$

In the present context, we can identify the entrance amplitude $V_{\vec{a}}(\vec{Q})$ with the matrix element that appears in Eq. (31),

$$V_{\vec{a}}(\vec{Q}) = \langle\tilde{\Psi}^{\mathrm{res}}|V|\vec{k}\Psi_o\rangle, \tag{33}$$

and use the partial-wave expansion of a plane wave

$$e^{i\vec{k}\cdot\vec{r_e}} = 4\pi\sum_{lm} i^l j_l(kr_e)Y_{lm}(\hat{r_e})Y^*_{lm}(\hat{k}) \tag{34}$$

to obtain

$$V_{\vec{a}}(\vec{Q}) = \frac{1}{\sqrt{2\pi}}\sum_{l,m} i^l 2\sqrt{k}\langle\tilde{\Psi}^{\mathrm{res}}|V|\Psi_o j_l Y_{lm}\rangle Y^*_{lm}(\theta,\zeta)$$

$$\equiv \frac{1}{\sqrt{2\pi}}\sum_{l,m} i^l \gamma_{lm}(\vec{q_{\mathrm{int}}})Y^*_{lm}(\theta,\zeta), \tag{35}$$

where the replacement of $Y_{lm}(\hat{k})$ by $Y_{lm}(\theta,\zeta)$ follows from choosing the body-fixed z-axis parallel with $\vec{R}$, and the space-fixed axis parallel with $\hat{k}$.

The usual argument for a narrow resonance [35], coupled with the fact that the scattering matrix must be unitary, leads to the constraint

$$\int d\bar{\Omega}|V_{\vec{a}}(\vec{Q})|^2 = \frac{1}{2\pi}\sum_{l,m}|\gamma_{lm}(\vec{q_{\mathrm{int}}})|^2 = \frac{\Gamma(\vec{q_{\mathrm{int}}})}{2\pi}, \tag{36}$$

which identifies $|\gamma_{lm}(\vec{q_{\mathrm{int}}})|^2$ as the partial resonance width associated with the angular momentum channel lm. In other words, the resonance amplitudes γ_{lm} suffice to completely determine the entrance amplitude $V_{\vec{a}}$ for a narrow resonance.

To obtain the amplitudes γ_{lm} at a given geometry, we carry out a multichannel resonance analysis of the quantities obtained from complex Kohn scattering calculations. For this purpose, it is convenient to work with the S-matrix rather than the T matrix:

$$T = \frac{S-1}{2i}. \tag{37}$$

The S-matrix for multichannel scattering near a resonance pole may be factored into background and resonant components as [35]

$$S = S^{\mathrm{bg}} \times S^{\mathrm{res}} = S^{\mathrm{bg}} \times \left(1 - \frac{iA}{E - E_R + i\Gamma/2}\right), \tag{38}$$

where A is an energy-independent matrix. Unitarity of S^{res} requires A to be Hermitian. Equation (38) can also be written

$$S = S^{\mathrm{bg}} - \frac{iB}{E - E_R + i\Gamma/2}, \tag{39}$$

where

$$B = S^{\mathrm{bg}}A \tag{40}$$

or

$$A = S^{\mathrm{bg}\dagger}B. \tag{41}$$

It can be shown [35] that if the resonance is nondegenerate, A and B are rank 1 matrices. Since A is also Hermitian, we can write

$$A_{lm,l'm'} = \delta_{lm}\delta^*_{l'm'}, \tag{42}$$

$$B_{lm,l'm'} = \gamma_{lm}\delta^*_{l'm'}, \tag{43}$$

where γ_{lm} and δ_{lm} satisfy

$$\sum_{l,m}|\gamma_{lm}|^2 = \sum_{l,m}|\delta_{lm}|^2 = \Gamma. \tag{44}$$

Since the system is time-reversal invariant, the S-matrix, as well as its residue at $E = E_R - i\Gamma/2$, must also be symmetric. This in turn requires B to be a symmetric matrix. In that case we can adjust the phases of γ_{lm} and δ_{lm} so that

$$\gamma_{lm} = \delta^*_{lm}, \tag{45}$$

and hence

$$B_{lm,l'm'} = \gamma_{lm}\gamma_{l'm'}. \tag{46}$$

Since A is a rank 1 matrix, it can have only one nonzero eigenvalue, λ, and corresponding normalized eigenvector or "eigenmode" $\vec{u}$ with components u_{lm}. In view of Eq. (42) and Eq. (44), it is clear that $\lambda = \Gamma$ and that $u_{lm} = \delta_{lm}/\sqrt{\Gamma}$, within an overall phase.

We can summarize these results by observing that the *resonant* portion of the T-matrix is described by a single eigenmode $\vec{u}$,

$$T^{\mathrm{res}}_{lm,l'm'} = -u^*_{lm}\frac{\Gamma}{2(E - E_R + i\Gamma/2)}u^*_{l'm'} \tag{47}$$

and that the components of the eigenmode $\vec{u}$ are the complex conjugates of the resonance amplitudes divided by $\sqrt{\Gamma}$,

$$u_{lm} = \gamma^*_{lm}/\sqrt{\Gamma}. \tag{48}$$

In our calculations, we first obtain Γ from a fit to the S_{p_x,p_x} matrix element, and then fit every matrix element of S independently to the linear form given by Eq. (39), using Γ in the denominator, thereby obtaining the coefficient matrices which we will call $S^{\mathrm{bg}\,1}$ and B^1. Then

$$A^1 = S^{\mathrm{bg}1\dagger} B^1. \tag{49}$$

We then construct the Hermitian part of A^1,

$$A_H = \tfrac{1}{2}(A^{1\dagger} + A^1), \tag{50}$$

and obtain its eigenvalues and eigenvectors. If Eq. (42) applies then of course there is only one nonzero eigenvalue; in practice, there were usually several eigenvalues with magnitudes $\sim 5\%$ that of the largest. We therefore took $\vec{u}$ to be the complex conjugate of the eigenvector whose eigenvalue is greatest in magnitude and used Eqs. (38), (42), and (48) to reconstruct the S-matrix. This procedure usually yielded RMS errors in the matrix elements of less than 10%.

We note that the coordinate system upon which the Y_{lm}'s of the scattering calculation were based was different from the one appropriate to the present analysis, oriented about the dissociative R axis. Therefore we performed a rotation of the amplitudes according to

$$\gamma_{lm} \rightarrow \sum_{m'} D^J_{m'm}(\alpha,\beta,\gamma)\gamma_{lm'}, \tag{51}$$

where $D^J_{m'm}$ is a Wigner rotation matrix and α,β,γ are the Euler angles which orient the coordinate system with $\hat{R}$ parallel to $\hat{z}$ with respect to the coordinate system of our scattering calculation.

In terms of the resonant eigenmode $\vec{u}$, the entrance amplitude [see Eq. (35)] may be expressed as

$$V_{\vec{a}}(\vec{Q}) = \sqrt{\frac{\Gamma(\vec{q}_{\mathrm{int}})}{2\pi}} \sum_{l,m} i^l u_{lm}(\vec{q}_{\mathrm{int}}) Y^*_{lm}(\theta,\zeta). \tag{52}$$

Applying the constant-eigenmode assumption of Eq. (24), but now for a polyatomic, the entrance amplitude is approximated as

$$V_{\vec{a}}(\vec{Q}) \approx V_{\mu_0}(\vec{q}_{\mathrm{int}}) y_{\mu_0}(\Omega_k) = V_{\mu_0}(\vec{q}_{\mathrm{int}}) y_{\mu_0}(\theta,\zeta). \tag{53}$$

In view of Eq. (52), we see that this approximation follows from the assumption that the coefficients u_{lm} do not vary with the internal nuclear coordinates of the target over the Franck-Condon region. In that case, we can define

$$V_{\mu_0}(\vec{q}_{\mathrm{int}}) = \sqrt{\frac{\Gamma(\vec{q}_{\mathrm{int}})}{2\pi}} \tag{54}$$

and

$$y_{\mu_0}(\theta,\zeta) = \sum_{l,m} i^l u_{lm}(\vec{q}_0) Y^*_{lm}(\theta,\zeta), \tag{55}$$

where we evaluate u_{lm} at the equilibrium geometry of the neutral, $\vec{q}_{\mathrm{int}} = \vec{q}_0$. The function $y_{\mu_0}(\theta,\zeta)$ then determines the angular dependence of the DEA cross section via Eq. (27). If the constant-eigenmode approximation does not apply, then the entrance amplitude can be evaluated using Eq. (52) and the differential DEA cross section is obtained by solving the LCP equation.

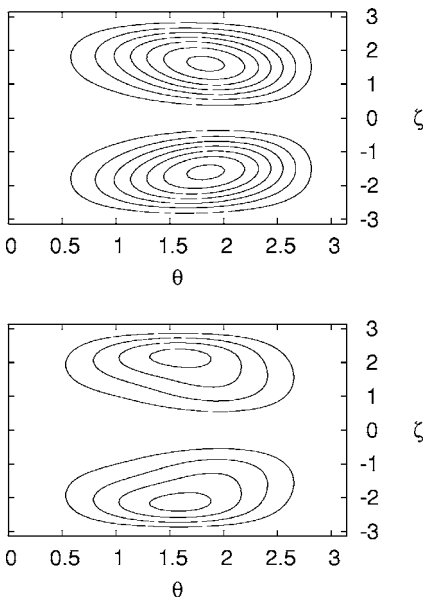

FIG. 3. Modulus-squared of the entrance amplitude $|V_{\vec{a}}|^2$ for the H_2O^- $^2B_1$ state at geometries $(r_1,r_2,\theta)=(1.81°,1.81°,104.5°)$ and (1.81°, 2.11°, 104.5°), internormalized; bond lengths, units of a_0, where $1a_0 = 5.291\,772\,1 \times 10^{-11}$ m.

VI. ANGULAR DISTRIBUTION OF H^-+OH

For the $^2B_1$ state of H_2O^-, the value of $|V_{\vec{a}}(\vec{q}_{\mathrm{int}},\theta,\zeta)|^2$ at the geometries $\vec{q}_{\mathrm{int}} = (r_1,r_2,\theta_{\mathrm{HOH}}) = (1.81a_0, 1.81a_0, 104.5°)$ and $(1.81a_0, 2.11a_0, 104.5°)$ is plotted in Fig. 3 with respect to the second and third Euler angles θ and ζ. The bond length r_1 is the nondissociative bond length. Although the overall magnitude at these geometries is different, the shape is clearly similar. The first geometry is the equilibrium geometry of water while the $(1.81a_0, 2.11a_0, 104.5°)$ result represents the greatest deviation from the equilibrium geometry result within the Franck-Condon region of the neutral.

In Fig. 4 the phase of the entrance amplitude is shown,

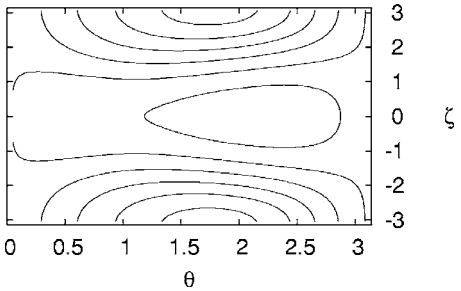

FIG. 4. Phase of the entrance amplitude $V_{\vec{a}}$ for the H_2O $^2B_1$ state, at geometry $(r_1,r_2,\theta_{\mathrm{HOH}})=(1.81,1.81,104.5)$, contours every 0.157 radians. Bond lengths, units of a_0.

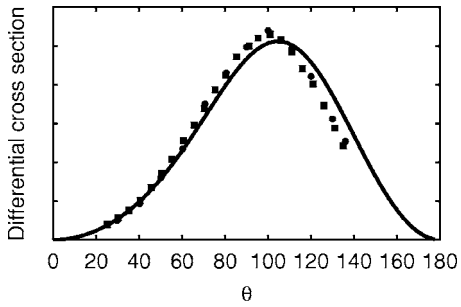

FIG. 5. Angular distribution of H^- from H^-+OH via dissociative attachment to the $^2B_1$ state, assuming axial recoil, along with the measurements of Belić, Landau, and Hall [10] (squares) and Trajmar and Hall [9] (circles), arbitrary units.

defined to be between $-\frac{\pi}{2}$ and $+\frac{\pi}{2}$, i.e., modulo π. With this definition the phase is symmetric under $\zeta \rightarrow -\zeta$, although due to the B_1 symmetry of the state the entrance amplitude is antisymmetric with respect to this operation. In a single-partial-wave approximation, there would be no variation in phase of the entrance amplitude with respect to the Euler angles θ and ζ, because the entrance amplitude would be proportional to a real spherical harmonic in θ and ζ times an overall phase. Thus, the deviations from zero apparent in this figure are due to the mixing of multiple partial waves into the entrance amplitude, with unequal phases. In particular, in the present case there is significant d-wave character mixed with the dominant p wave.

The relative constancy of the shape of the angular dependence of the entrance amplitude is consistent with Eq. (24) and with the observation [10] that the angular distribution for this process does not vary noticeably with final state.

The angular dependence which we have calculated as per Eq. (27) is plotted in Fig. 5, along with experimental data [9,10]. For this calculation we used complex Kohn results from the equilibrium geometry of $r_1=r_2=1.81a_0$, $\theta_{\mathrm{HOH}}=104.5°$. Continuum basis functions with l up to 5 were included in this calculation. The total width was 0.010 89 eV [from denominator of Eq. (39)] or 0.012 55 eV (the largest eigenvalue of A_H).

This result is different from the value of 0.006 eV which we obtained earlier [1] using a similar calculation. Our orbital basis for the present calculation consisted of the $1a_1, 2a_1, 1b_2, 3a_1, 1b_1$ plus a correlating a' orbital from a multiconfiguration self-consistent-field (MCSCF) calculation on the neutral, as well as $4a_1, 2b_2, 5a_1, 2b_1$ orbitals from an MCSCF calculation on the resonance. Our configuration space consisted of a full configuration interaction (CI) in the six neutral orbitals, with the $1a_1$ and $2a_1$ orbitals always doubly occupied, plus double excitations into the resonance orbital space. In our earlier calculations, we omitted the correlating a' orbital for the neutral and the $2b_1$ resonance orbital, and used natural orbitals from CI calculations on the resonance and neutral for the rest; the configuration space for the target and scattering calculations was full CI in the eight orbitals, with the 1 and $2a_1$ orbitals doubly occupied. We do not have a simple explanation for the discrepancy in widths, other than the speculation that in the present case the width may have been enhanced by coupling through the $2b_1^1$ shape resonance configuration to the continuum.

VII. ANGULAR DISTRIBUTION OF H^-+SH

For dissociative attachment to H_2S via the $^2B_1$ resonance state, the angular dependence of the cross section is itself dependent upon the final vibrational state of the SH fragment. As a result, we must perform nuclear dynamics calculations to resolve the different vibrational states produced at each orientation θ, in order to evaluate the angular dependence of Eq. (19) with the help of the axial recoil approximation.

A. Entrance amplitude

The $^2B_1$ resonance state of H_2S is even narrower than its H_2O counterpart. From complex Kohn calculations, we obtain a width of 0.003 318 eV [from denominator of Eq. (39)] or 0.003 611 eV (largest eigenvalue of A_H) at the equilibrium geometry of the neutral.

For these calculations, we treated the electronic N- and $(N+1)$-electron Hamiltonians of H_2S+e^- in a nonrelativistic fashion with all electrons included. Inclusion of relativistic corrections is undoubtedly important for a fully faithful reproduction of the electronic properties of sulfur-containing compounds; however, the object of this study was only to reproduce the qualitative features of the experiment, and the simple nonrelativistic treatment was sufficient to do so, albeit imperfectly.

On the sulfur atom, we used the double-zeta s and p basis set of Dunning [36] along with d functions with exponents 0.5, 0.0866, and 0.015; p functions with exponents 0.041 and 0.02; and an s function with exponent 0.023. On the hydrogen, we used the basis of Gil *et al.* [14] plus an s function with exponent 0.007 250, and a p function with exponent 0.027 35, for a total of 69 contracted Gaussian basis functions. We used this basis to obtain five a_1, two b_1, and two b_2 orbitals from a self-consistent-field calculation on neutral H_2S. We calculated eight a_1, one a_2, two b_1, and four b_2 singlet-coupled improved virtual orbitals (IVOs) [37] in the field of the $^2B_1$ grandparent. For the scattering calculation eight of the nine SCF orbitals were kept doubly occupied; the remaining $2b_1$ orbital was included with the 15 IVOs, and this set comprised the active space for two- and three-electron full CI calculations defining the target and Q-space configurations of the scattering calculation, respectively. We included l up to 6 for the continua.

We obtained amplitudes γ_{lm} at 100 points, comprising the grid of $r_1, r_2=\{2.13, 2.33, 2.53, 2.73, 2.93a_0\}$, $\theta_{\mathrm{HSH}}=\{72°, 92°, 112°, 132°\}$. It was not necessary to perform the scattering calculation for both $(r_1, r_2, \theta)=(A, B, C)$ and (B, A, C); to obtain the entrance amplitude for the latter, a reflection was performed in addition to the rotations of Eq. (51). It is important to note that while the total width and partial width into each l are independent of the coordinate system and thus equal for the (A, B, C) and (B, A, C) geometries, the amplitudes will be different, because we choose the $\hat{z}$ axis to be parallel to r_2 ("the dissociative bond length") and not r_1 ("the nondissociative bond length"). To obtain a global representation of each $u_{lm}(\vec{q}_{\mathrm{int}})$, we fit its value at the 100 calculated points to a polynomial in r_1, r_2, and $\cos(\theta)$,

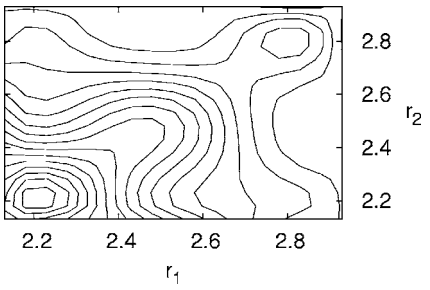

FIG. 6. Total width Γ of $^2B_1$ state of H_2S^- at $\theta_{HSH}=92°$, contours every 4×10^{-4} eV, where 1 eV=1.602 176 5$\times10^{-19}$ J.

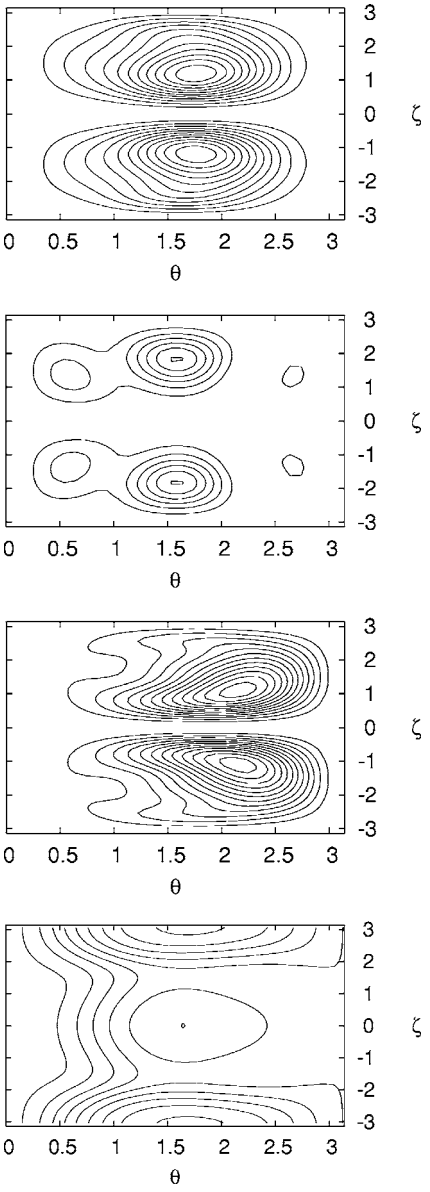

FIG. 7. Top to bottom: Modulus-squared of the entrance amplitude $|V_{\bar{a}}|^2$ for the H_2S^- $^2B_1$ state at geometries $(r_1,r_2,\theta_{HSH})=(2.53°,2.53°,92°)$, (2.13, 2.93, 92°), and (2.53, 2.13, 92°), internormalized. Bond lengths, units of a_0. Bottom panel, phase of entrance amplitude $V_{\bar{a}}$ at (2.53°, 2.53°, 92°), contours every 0.157 radians.

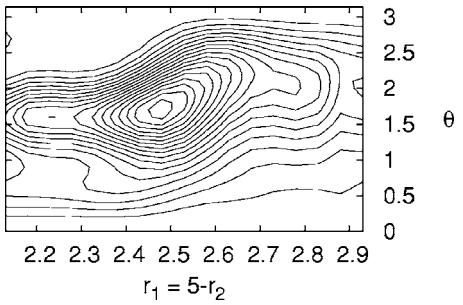

FIG. 8. Dependence of $\int d\zeta|V_{\bar{a}}|^2$ upon asymmetric stretch (in units of a_0) and Euler angle θ, at $r_1+r_2=5a_0$, $\theta_{HSH}=92°$, arbitrary units.

fourth order in the bond lengths and cubic in $\cos(\theta)$.

We find that the total width is peaked near the equilibrium geometry of the neutral, which is $(r_1,r_2,\theta_{HSH})=(2.53a_0,2.53a_0,92°)$, and also increases as both r_1 and r_2 get smaller. A plot of the total width is shown in Fig. 6. Some of the irregularity in this figure is due to the polynomial fit. In Fig. 7 the modulus-squared of the entrance amplitude is plotted for the equilibrium geometry (top) and others; it is clearly not factorable as per Eq. (24), as its shape changes from panel to panel. At the bottom in Fig. 7 is plotted the phase of the entrance amplitude at the equilibrium geometry of the neutral, which varies more than does the phase for the H_2O^- state (Fig. 4).

Figures 8 and 9 demonstrate what we believe to be the main cause of the final-state-specific angular dependences in H_2S. In Fig. 8 the symmetric stretch coordinate r_1+r_2 is held constant at $5a_0$, the bond angle θ_{HSH} is held at 92°, and the dependence of $\int d\zeta|V_{\bar{a}}|^2$ with respect to the Euler angle θ and asymmetric stretch distance is plotted. The coordinate r_1 is the nondissociative bond length (equal to the Jacobi coordinate r).

At large θ, the $\hat{R}$ axis which points toward the dissociating H^- is oriented back toward the incident electron source. At this orientation, the entrance amplitude is insignificant for values of $r_1<r_2$, as can be seen in Fig. 8, and this behavior will be reflected in the initial nuclear wave packet, as is clear in Fig. 9. This figure shows the initial wave packet for the dominant $\Lambda=1$ component of the entrance amplitude $V_{\bar{a}}$,

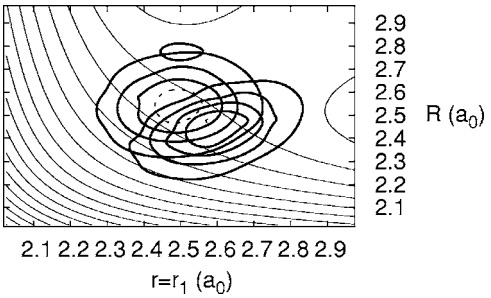

FIG. 9. Square of driving term $|\phi_{\nu_i}|^2$ for initial wave packet, normalized to unity, $\Lambda=1$ calculation, integrated over Jacobi angle γ, for $\theta=45°$ (circular) and 165° (oblong) calculations, with potential energy surface at $\gamma=92°$, contours every 0.25 eV. Distances in units of a_0.

$$V_{\bar{a}} = \sum_{\Lambda} V_{\Lambda}(r,R,\gamma,\theta)\frac{e^{i\Lambda\zeta}}{\sqrt{2\pi}}, \tag{56}$$

for back-scattering of the H^- at $\theta=165°$ (oblong) and forward scattering at $\theta=45°$ (more circular). The shape of the initial wave packet at $\theta=165°$ will lead to less vibrational excitation for large kinetic energy in the dissociative direction, relative to the calculation at $\theta=45°$. This is because for the $\theta=165°$ calculation, the parts of the initial wave packet at small initial r_2, which are higher up on the repulsive wall and thus will correspond to the components of the wave function exiting with large kinetic energy in the dissociative r_2 direction, have a relatively large expectation value $\langle r_1\rangle$, which means that these components will experience a smaller impulse in the vibrational r_1 coordinate at the beginning of the dissociation.

B. Potential energy surface

Because the $^2B_1$ resonance state of H_2S is so narrow, the real part of its energy is well represented (though not variationally) by bound-state computational methods. We therefore carried out CI calculations for the resonance state, using an effective core potential on the sulfur atom to replace the n equals 1 and 2 inner-shell electrons; we used the potential parameters and the corresponding primitive basis given by Pacios and Christiansen [38], the latter augmented with d functions with exponents 0.819, 0.269, 0.101, and 0.037 92. On the hydrogen, we used the basis of Gil *et al.* [14] plus s functions with exponents 0.007 250 and 0.001 767, and a p function with exponent 0.027 35. We used this primitive basis to obtain MCSCF orbitals for the resonance state. The MCSCF calculation included the dominant $2b_1^{-1}\,6a_1^2$ configuration of the resonance plus the two correlating excitations $6a_1^2 \rightarrow 7a_1^2, 3b_2^2$. We then performed a CI calculation with all single and double excitations out of these configurations, keeping the $2b_1$ orbital occupancy at 0 or 1. We performed this calculation at several points and fit the result to a modified extended LEPS potential [39] plus Gaussian function,

$$\begin{aligned} V = {} & \frac{Q_{r_1}}{1-0.5381} + \frac{Q_{r_2}}{1-0.5381} + \frac{Q_{r_{\mathrm{HH}}}}{1-0.1814} \\ & - \sqrt{0.5\left(\alpha + 0.055\,32^2 \exp\frac{-\alpha}{0.055\,32^2}\right)} - 10.944\,195 \\ & - 0.004\,329\cos(\theta_{\mathrm{HSH}}) - 0.001\,414\cos(2\theta_{\mathrm{HSH}}) \\ & - 0.000\,2454\cos(3\theta_{\mathrm{HSH}}) + \exp(-0.3011b)[-0.6380 \\ & + 0.2041\cos(\theta_{\mathrm{HSH}}) + 0.2296\cos(2\theta_{\mathrm{HSH}}) \\ & + 0.1227\cos(3\theta_{\mathrm{HSH}})], \end{aligned} \tag{57a}$$

$$b = (r_1^{7.552} + r_2^{7.552})^{2/7.552}, \tag{57b}$$

$$\begin{aligned} \alpha = {} & \frac{(J_{r_1} - J_{r_2})^2}{(1-0.5381)(1-0.5381)} + \frac{(J_{r_2} - J_{r_{\mathrm{HH}}})^2}{(1-0.5381)(1-0.1814)} \\ & + \frac{(J_{r_1} - J_{r_{\mathrm{HH}}})^2}{(1-0.5381)(1-0.1814)}, \end{aligned} \tag{57c}$$

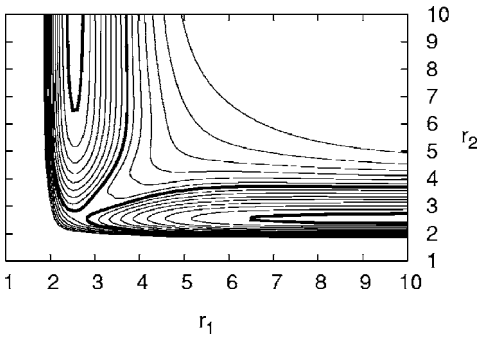

FIG. 10. Fitted H_2S potential surface at $\theta_{\mathrm{HSH}}=92°$, with contours every 0.25 eV. Bond lengths in units of a_0.

$$\begin{aligned} Q_{r_1} &= 0.1076(0.75M_{r_1}^2 - 0.5M_{r_1}), \\ J_{r_1} &= 0.1076(0.25M_{r_1}^2 - 1.5M_{r_1}), \\ M_{r_1} &= \exp - 0.8728(r_1 - 2.4587), \\ Q_{r_2} &= 0.1076(0.75M_{r_2}^2 - 0.5M_{r_2}), \\ J_{r_2} &= 0.1076(0.25M_{r_2}^2 - 1.5M_{r_2}), \\ M_{r_2} &= \exp - 0.8728(r_2 - 2.4587), \\ Q_{r_{\mathrm{HH}}} &= 0.4147(0.75M_{r_{\mathrm{HH}}}^2 - 0.5M_{r_{\mathrm{HH}}}), \\ J_{r_{\mathrm{HH}}} &= 0.4147(0.25M_{r_{\mathrm{HH}}}^2 - 1.5M_{r_{\mathrm{HH}}}), \\ M_{r_{\mathrm{HH}}} &= \exp - 0.1812(r_{\mathrm{HH}} + 8.0119). \end{aligned} \tag{57d}$$

This potential is plotted at $\theta_{\mathrm{HSH}}=92°$ in Fig. 10.

Our previous calculations on the $^2B_1$ state of H_2O^- indicated that only a few percent of the propagating wave packet was lost to autodetachment. Because the $^2B_1$ state of H_2S^- has an even smaller width, and because the real parts of the potential energy surfaces are similar for these states, we did not include the imaginary component $\frac{-i\Gamma}{2}$ in the Hamiltonian when carrying out the time propagation. We expect this omission in the present calculation to have a negligible effect.

To obtain the initial H_2S vibrational wave packet χ_{v_i}, a neutral potential energy surface was required. We used the surface of Senekowitch *et al.* [40]. We adjusted the zero of energy to match the result of a single CI calculation at the equilibrium geometry of the neutral. This CI calculation used the same primitive basis and pseudopotential as the resonance CI calculation, and was defined by the SCF configuration plus all single and double excitations.

These two CI calculations yield a vertical excitation energy of 0.217 03 hartrees or 5.906 eV for the resonance.

C. Triatomic coordinate system and Hamiltonian

For the nuclear dynamics calculations, the internal coordinates $\vec{q}_{\mathrm{int}}$ are defined to be the Jacobi coordinate system R,

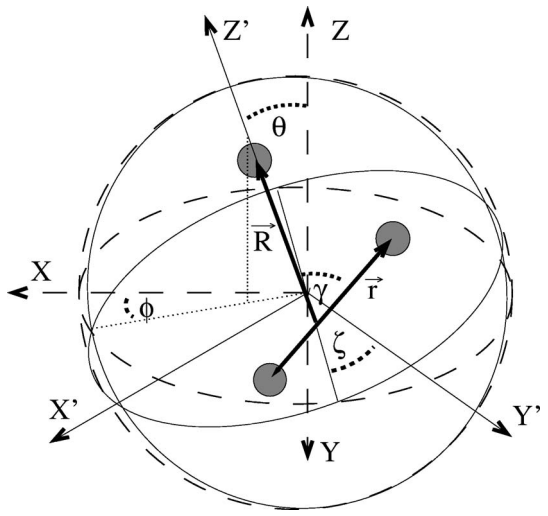

FIG. 11. "*R*-embedding" coordinate system used in this calculation. The origin is the center of mass. The body-fixed (BF) frame is labeled by the X', Y', and Z' axes; the space-fixed (SF), by X, Y, and Z. The BF axes are marked with thin lines, and the BF $X'Z'$ and $X'Y'$ planes are both marked with a thin line circle. The SF axes are marked with dashed lines, and the SF XZ and XY planes are marked with dashed circles. The molecule resides in the BF $X'Z'$ plane. The Euler angles ϕ, θ, and ζ orient the BF frame with respect to the SF frame. The line of nodes is also drawn. The $\vec{r}$ vector connects the nuclei of the diatomic. The $\vec{R}$ vector connects the center of mass of the diatomic to the third atom and is collinear with the BF Z' axis. R is the length of $\vec{R}$, r is the length of $\vec{r}$, and γ is the angle between the $\vec{R}$ and $\vec{r}$ vectors.

r, and γ. Specifically, r is the distance between one H and the S; R is the distance between the center of mass of that SH diatomic and the second H; and γ is the angle between the R and r vectors such that $\gamma=0$ denotes a linear SHH configuration.

The three remaining degrees of freedom of the center-of-mass system are the Euler angles which define the orientation of the body-fixed (BF) frame with respect to the space-fixed (SF) frame. We continue to use the "R-embedding" [34] coordinate system and thus define ϕ and θ to be the polar angles which orient the R vector with respect to the SF frame, and ζ as the third Euler angle specifying orientation about the BF z axis (parallel with $\hat{R}$), just as in Fig. 2. This coordinate system is shown in full detail in Fig. 11.

We will denote by J the total angular momentum quantum number and by M the quantum number about the space-fixed z axis, parallel with the wave vector of the incident electron. These quantum numbers are conserved by the Hamiltonian. The six-dimensional rovibrational wave function for a triatomic with specified J and M value can be expanded as follows:

$$\chi_{\nu_i}(R,r,\gamma,\phi,\theta,\zeta)=\sum_K \tilde{D}^J_{MK}(\phi,\theta,\zeta)\frac{\chi^K_{\nu_i}(R,r,\gamma)}{Rr}, \quad (58)$$

where the basis of $\tilde{D}^J_{MK}(\phi,\theta,\zeta)$ is the set of normalized Wigner rotation matrices (and BF angular momentum eigenstates),

$$\tilde{D}^J_{MK}(\phi,\theta,\zeta)=\sqrt{\frac{2J+1}{8\pi^2}}D^J_{MK}(\phi,\theta,\zeta)$$
$$=\sqrt{\frac{2J+1}{8\pi^2}}d^J_{MK}(\theta)e^{iM\phi}e^{iK\zeta}, \quad (59)$$

such that

$$\int_0^{2\pi}d\phi\int_{-1}^{1}d(\cos\theta)\int_0^{2\pi}d\zeta$$

$$\tilde{D}^J_{MK}(\phi,\theta,\zeta)\tilde{D}^{J'*}_{M'K'}(\phi,\theta,\zeta)=\delta_{J,J'}\delta_{M,M'}\delta_{K,K'}. \quad (60)$$

We will also define for convenience a normalized d^J_{MK},

$$\tilde{d}^J_{MK}(\theta)=\sqrt{\frac{2J+1}{2}}d^J_{MK}(\theta). \quad (61)$$

In Eqs. (59)–(61) we follow the conventions of Zhang [41], which for the D^J_{MK} is the same as that of Edmonds [42].

In Ref. [2], we employed the standard [43,44] BF Hamiltonian for the radial solutions $\chi^K_{\nu_i}$ of this expansion,

$$H^J_{KK}=-\frac{1}{2\mu_R}\frac{\partial^2}{\partial R^2}-\frac{1}{2\mu_r}\frac{\partial^2}{\partial r^2}+\frac{\hat{j}^2}{2\mu_r r^2}$$
$$+\frac{1}{2\mu_R R^2}[J(J+1)-2K^2+\hat{j}^2]+V(R,r,\gamma),$$

$$H^J_{K\pm1,K}=-\frac{1}{2\mu_R R^2}\sqrt{J(J+1)-K(K\pm1)}\hat{j}_\pm$$

$$\hat{j}^2=-\left(\frac{1}{\sin\gamma}\frac{\partial}{\partial\gamma}\sin\gamma\frac{\partial}{\partial\gamma}-\frac{K^2}{\sin^2\gamma}\right),$$

$$\hat{j}_\pm=\mp\frac{\partial}{\partial\gamma}-K\cot(\gamma), \quad (62)$$

where μ_r and μ_R are the reduced masses in either direction and V is the Born-Oppenheimer potential energy surface which we calculate.

D. Implementation

The interested reader is referred to the Appendix for a complete derivation of the working equations, which employ the axial recoil approximation.

We expand $V_{\bar{a}}$ as per Eq. (56), and calculate cross sections using the expression

$$\frac{\partial\sigma^{\nu}_{\mathrm{DEA\ exp't}}}{\partial\Omega_k}=\lim_{R\to\infty}\frac{2\pi\kappa_\nu}{\mu_R k^2}\times\sum_\Lambda\int d(\cos\gamma)$$
$$\times\left|(\chi_\nu|\hat{g}^+_{00}|V_\Lambda(\theta)\chi_{\nu_i})\right|^2. \quad (63)$$

The Green's function $\hat{g}^+_{00}$ corresponds to the Hamiltonian with $J=0$, $K=0$ in Eq. (62). Thus, at each desired angle θ, we perform one calculation for each value of Λ, the number of quanta of K-excitation (excitation of the projection of angu-

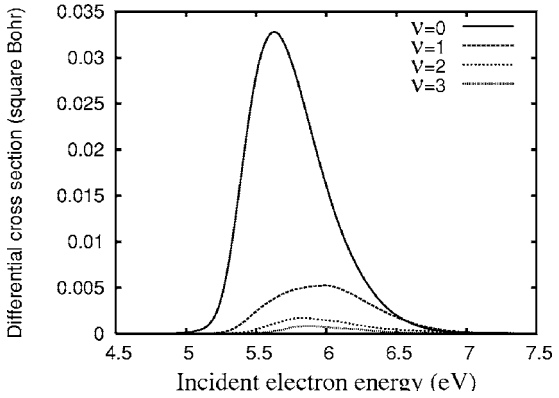

FIG. 12. Differential cross section for $H^-+SH(\nu)$ from H_2S at scattering angle $\theta=45°$, arbitrary units.

lar momentum upon the body-fixed $\hat{R}$ vector) imparted by the entrance amplitude, and sum the cross sections produced.

The evaluation of the limit in Eq. (63) is performed within the MCTDH package [33], and is calculated at $R=9$ to $12a_0$. Further details can be found in Ref. [2].

In Fig. 9 we have shown the initial wave packet for calculations at $\theta=45°$ and 165°. The difference between these wave packets is readily apparent. The differential cross sections at these two angles are plotted in Figs. 12 and 13, respectively, as a function of incident electron energy for different final vibrational states of HS. These differential cross sections, while given in arbitrary units, are internormalized. The calculations show that at energies above 6.25 eV, the cross section for producing HS in its ground vibrational state clearly dominates at $\theta=165°$, while at the same energies for $\theta=45°$, the cross sections for producing HS in $\nu=0$ and $\nu=1$ are comparable.

Our calculated results are consistent with the findings of Azria *et al.* [17], though not quantitatively. These authors found that at large scattering angles θ and within the high energy tail of the dissociative attachment cross section, the ground vibrational state dominates. They found that as the scattering angle is decreased, the branching ratio between the ground and first excited vibrational state decreases until at 45°, the first excited vibrational state actually dominates the first. Again, we are still referring only to the high energy tail of the DEA cross section. Although our results do not indicate that the first excited vibrational state is ever clearly dominant, it is apparent that the basic trend observed in the experiments of Azria *et al.* [17] is reflected by these calculations.

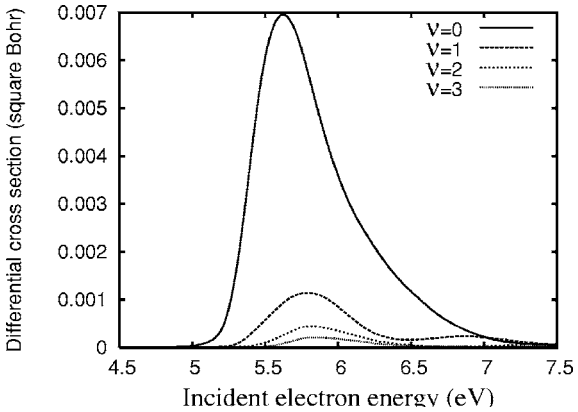

FIG. 13. Differential cross section for $H^-+SH(\nu)$ from H_2S at scattering angle $\theta=165°$, arbitrary units.

VIII. DISCUSSION

A formalism for studying the angular dependence of dissociative electron attachment, which was originally given for diatomic targets by O'Malley and Taylor [24], is extended here to polyatomic targets. A central part of the treatment is the assumed validity of the axial recoil approximation, which states that the vector $\vec{R}$, the asymptotic orientation of which defines the scattering angle of the dissociating fragments relative to the incident electron direction, in fact does not change orientation at all during the course of the collision. For diatomic targets, the axial recoil approximation applies whenever the kinetic energies involved in the dissociation are much larger than the centrifugal energy terms over the entire range of populated rotational levels. For polyatomic targets, the situation is more complicated and the validity of the axial recoil approximation also depends on the shape of the anion potential energy surface over the region sampled in the dissociation. The agreement between our calculated results and experiment can be taken as supporting our finding that the potential energy surfaces of both resonances studied vary weakly with the Jacobi angle γ in the inner region, at least for the geometries sampled by the propagating wave packet.

The dissociative attachment cross section is determined by the asymptotic form of the solution of a inhomogeneous nuclear wave equation, which we treat here in the local complex potential model. The angular dependence of this solution ξ_{ν_i} depends upon the angular dependence of its driving term ϕ_{ν_i}, which in turn depends upon that of the entrance amplitude $V_{\bar{a}}$. When the functional dependence of the entrance amplitude on the internal nuclear target coordinates can be factored from its dependence on the Euler angles which orient the target in space—a situation we have termed the constant-eigenmode approximation—then the angular dependence of the DEA cross section is independent of the vibrational level of the final state. If, in addition, the axial recoil approximation applies, then we have shown that the angular dependence of the cross section can be determined solely from an analysis of the electronic entrance amplitude for fixed nuclear geometry and a numerical solution of the nuclear wave equation is not needed.

This was found to be the case for water. The angular distribution we have obtained for H_2O is in excellent agreement with experiment [9,10]. Moreover, our analysis shows that the asymmetry in the distribution, which is peaked near 100 degrees, results from the mixing of partial waves in the resonant electronic T-matrix and not, as had been suggested [10], from distortion of the incident electron plane wave caused by direct scattering. Whereas a pure p-wave resonance would lead to a symmetric, $(1-\cos^2\theta)$ angular distribution, the presence of d-waves mixed in with the dominant

p-wave component weights the entrance amplitude toward the negative end of the H_2O dipole moment (the oxygen side, not the hydrogen side). This in turn leads to the dissociative nuclear wave packet being preferentially oriented with the dissociative hydrogen pointing in the backwards direction ($\theta > 90°$). It is interesting to consider that in this case the angular distribution of dissociative attachment may be reflecting the underlying shape of the $1b_1$ orbital, one electron from which must be excited into the $4a_1$ orbital to achieve the $^2B_1$ Feshbach resonance configuration $[H_2O]1b_1^{-1}4a_1^2$. The $1b_1$ orbital is the lone pair orbital in H_2O, and is mostly oxygen $2p_x$, but has some d-wave character as well.

For the case of H_2S, we have shown that the dependence on internal coordinates cannot be factored from the entrance amplitude, which in turn leads to a dependence of the angular distribution on the final vibrational state of HS that is detected. By solving the nuclear wave equation in full dimensionality for different values of the scattering angle, we have confirmed the experimental findings of Azria *et al.* [17] that, for incident energies in the high energy tail of the DEA peak, the ground state of HS is preferentially produced at large scattering angles, whereas at 45 degrees the cross sections for production of HS in its ground and first excited vibrational levels are comparable.

ACKNOWLEDGMENTS

This work was performed under the auspices of the U.S. Department of Energy by the University of California Lawrence Berkeley National Laboratory under Contract No. DE-AC02-05CH11231. The work was supported by the US DOE Office of Basic Energy Science, Division of Chemical Sciences.

APPENDIX: AXIAL RECOIL APPROXIMATION

1. Diatomic case

We assume that the nuclear dynamics of the resonant state is described by the local complex potential model, Eq. (2), with an effective Hamiltonian H_a of the form

$$H_a = T_{\vec{Q}} + V(\vec{q}_{\text{int}}). \tag{A1}$$

The effective complex potential V is assumed to be local and to depend only on the internal nuclear degrees of freedom [24]. In the case of a diatomic, V depends only of the internuclear distance R, while the Hamiltonian takes the form

$$H = -\frac{1}{2\mu_R R^2}\left(\frac{\partial}{\partial R}R^2\frac{\partial}{\partial R} + \frac{1}{\sin\theta}\frac{\partial}{\partial\theta}\sin\theta\frac{\partial}{\partial\theta} + \frac{1}{\sin^2\theta}\frac{\partial^2}{\partial\phi^2}\right) + V(R). \tag{A2}$$

Since the rotational eigenfunctions are the spherical harmonics $Y_{jm}(\Omega_k)$, the Green's function has the representation [45]

$$G^+(\vec{Q};\vec{Q}';E) = \sum_{jm} Y_{jm}(\Omega_k) g_j^+(R;R';E) Y_{jm}^*(\Omega_k') = \sum_{jm} Y_{jm}(\Omega_k)\Xi_j^0(R_<)\frac{\mu_R}{\kappa R R'}\Xi_j^+(R_>)Y_{jm}^*(\Omega_k'), \tag{A3}$$

where the functions $\Xi_j^{0/+}$ are regular and outgoing solutions, respectively, of the radial Schrödinger equation

$$\left(-\frac{1}{2\mu_R}\frac{\partial^2}{\partial R^2} + \frac{j(j+1)}{2\mu_R R^2} + V(R) - \kappa^2/2\right)\Xi_j^{0/+}(R) = 0 \tag{A4}$$

that behave asymptotically as

$$\Xi_j^0(R) \underset{r\to\infty}{\sim} e^{i\delta_j}\sin(\kappa R - j\pi/2 - \delta_j),$$

$$\Xi_j^+(R) \underset{r\to\infty}{\sim} e^{i\kappa R}, \tag{A5}$$

where δ_j is a phase shift. For an absorptive V with a negative imaginary component, δ_j has a negative imaginary component, and Ξ^0 has net incoming wave character at large R.

The solution of the LCP equation [Eq. (9)] for the case of a diatomic can thus be written as

$$\xi_{\nu_i}(\vec{Q}) = \sum_{jm} Y_{jm}(\Omega_k) \times \int d^3R' g_j^+(R;R';E) Y_{jm}^*(\Omega_k')\phi_{\nu_i}(R',\Omega_k') = \sum_{jm} Y_{jm}(\Omega_k)\frac{\mu_r}{\kappa R} \times \int d^3R' \frac{\Xi_j^0(R_<)\Xi_j^+(R_>)}{R'} Y_{jm}^*(\Omega_k')\phi_{\nu_i}(R',\Omega_k'). \tag{A6}$$

The driving term ϕ_{ν_i} will generally include contributions from a limited range of j values. If the corresponding radial functions $\Xi_j^{0/+}$ vary slowly with j over this range, then $\Xi_j^{0/+}$ can be replaced by an effective $\Xi_{j_t}^{0/+}$ and the radial portions of integrals in Eq. (A6) can be taken outside the sum,

$$\xi_{\nu_i}(\vec{Q}) \approx \int d\Omega_k'\left(\sum_{jm} Y_{jm}(\Omega_k)Y_{jm}^*(\Omega_k')\right) \times \frac{\mu_r}{\kappa R}\int dR' \frac{\Xi_{j_t}^0(R_<)\Xi_{j_t}^+(R_>)}{R'}\phi_{\nu_i}(R',\Omega_k'). \tag{A7}$$

This replacement gives an effective delta function in the Green's function G^+, when it operates on ϕ_{ν_i},

$$\xi_{\nu_i}(\vec{Q}) = \int d\vec{Q}' G^+(\vec{Q};\vec{Q}';E)\phi_{\nu_i}(\vec{Q}')$$

$$\approx \int d^3R' g^+_{j_t}(R;R';E)\delta(\Omega_k - \Omega'_k)\phi_{\nu_i}(\vec{R}'). \quad \text{(A8)}$$

The delta function above results in the recoil staying along the original orientation axis. By assuming that the $\Xi_j^{0/+}$ do not change much among the relevant values of j, we are requiring that the kinetic energies involved in dissociation are much larger than the relevant centrifugal energies, i.e., that the centrifugal term in Eq. (A4) is negligible.

2. Polyatomic case

For a polyatomic, the situation is a bit more complicated, and the axial recoil approximation imposes more constraints upon the dissociation dynamics than it does for a diatomic. In particular, while for a diatomic target j and m_j are good quantum numbers, any polyatomic Hamiltonian [e.g., Eq. (62)] imposes coupling among the values of the quantum number K. And although one may write a polyatomic Hamiltonian using different angular momentum coupling schemes, all such forms introduce couplings between angular momentum quantum numbers that are problematic for the axial recoil approximation. For instance, the Hamiltonian may be written in terms of the uncoupled spherical harmonics $Y_{lm_l} \times Y_{jm_j}$. In this case (and unlike the diatomic case), there is coupling among various j and m_j values. The physical origin of the problematic coupling is the γ dependence of the potential $V(r,R,\gamma)$ which couples the angular momentum of the two fragments of the dissociative attachment process. As a result of this potential, a polyatomic molecule may undergo bending motion during dissociation which changes the orientation of the recoil axis from its original position in the bound state.

In order to eliminate the problematic coupling among angular momentum quantum numbers, an appropriate decoupling scheme or other approximation must be introduced. We use an approximation, alternatively called the centrifugal sudden or coupled-states (CS) approximation [46,47]. However, we stress that the treatment we invoke to deal with this problem is by no means unique. In particular, the infinite-order sudden (IOS) approximation [48] provides an alternate approach to a useful result, and has been used to calculate angular dependences in photodissociation. For the current system, however, we believe that the IOS approximation is not applicable, due to the long-range ion-dipole interaction of the fragments.

For a polyatomic molecule, the centrifugal sudden approximation entails the neglect of the off-diagonal coupling $H_{K,K\pm1}$. For the triatomic Hamiltonian of Eq. (62), the centrifugal sudden approximation is

$$H^{JK}_{\mathrm{CS}} = -\frac{1}{2\mu_R}\frac{\partial^2}{\partial R^2} - \frac{1}{2\mu_r}\frac{\partial^2}{\partial r^2} + \frac{\hat{j}^2}{2\mu_r r^2} + \frac{1}{2\mu_R R^2}[J(J+1) - 2K^2 + \hat{j}^2] + V(R,r,\gamma). \quad \text{(A9)}$$

Since the coupling term in Eq. (62) is proportional to $\hat{j}_\pm/R^2$, its neglect requires that, for small R, the effect of $\hat{j}_\pm$ on the propagating wave packet be small. This in turn requires that for small R the momentum in the γ direction be small (i.e., $\frac{\partial}{\partial\gamma}$ be small) and that the propagating wave packet not sample the region around $\gamma=0$ or $\gamma=180°$, where $\cot(\gamma)$ is infinite. Therefore, the initial wave packet must start at a nonlinear geometry at which the potential is relatively flat in γ, and only spread to $\gamma=0$ or $\gamma=180°$ after the dissociation is well under way. We have found that this is the case for the $^2B_1$ resonant states of both water and H_2S.

The CS approximation allows us to write, in analogy with Eq. (A3),

$$G^+ = \sum_{J,M,K} \tilde{D}^J_{MK}(\phi,\theta,\zeta)\tilde{D}^J_{MK}(\phi',\theta',\zeta')g^+_{J,K}(\vec{q}_{\mathrm{int}};\vec{q}'_{\mathrm{int}};E)$$

$$= \frac{1}{(2\pi)^2}\sum_{J,M,K} e^{iM\phi}e^{iK\zeta}e^{-iM\phi'}e^{-iK\zeta'}\tilde{d}^J_{MK}(\theta)\tilde{d}^J_{MK}(\theta') \times g^+_{J,K}(\vec{q}_{\mathrm{int}};\vec{q}'_{\mathrm{int}};E). \quad \text{(A10)}$$

Subsequently, we make the same assumption that we did in deriving the axial approximation for a diatomic and treat the centrifugal term in the CS Hamiltonian of Eq. (A10) in an approximate way, replacing J by an averaged quantity,

$$G^+ = \frac{1}{(2\pi)^2}\sum_K g^+_{J_t,K}(\vec{q}_{\mathrm{int}};\vec{q}'_{\mathrm{int}};E)e^{iK(\zeta-\zeta')} \times \sum_J \tilde{d}^J_{MK}(\theta)\tilde{d}^J_{MK}(\theta')\sum_M e^{iM(\phi-\phi')}$$

$$= \frac{1}{2\pi}\sum_K g^+_{J_t,K}(\vec{q}_{\mathrm{int}};\vec{q}'_{\mathrm{int}};E)e^{iK(\zeta-\zeta')} \times \delta(\Omega_k - \Omega'_k). \quad \text{(A11)}$$

The second identity in Eq. (A11) follows from the fact that the set $\tilde{d}^J_{MK}$ for fixed M and K are solutions of a Sturm-Louisville differential equation in $\cos(\theta)$,

$$\left[\frac{\partial}{\partial\cos\theta}\sin^2\theta\frac{\partial}{\partial\cos\theta} + \frac{1}{\sin^2\theta}(M^2 + K^2 - 2MK\cos\theta) - J(J+1)\right]\tilde{d}^J_{MK}(\theta) = 0, \quad \text{(A12)}$$

and are therefore complete in θ, meaning complete in the norm.

3. Axial recoil approximation with constant-eigenmode approximation for a polyatomic

For a polyatomic molecule, we make use of the constant-eigenmode approximation of Eq. (53) as follows. We expand the associated angular function y_{μ_0} as

$$y_{\mu_0}(\theta,\zeta) = \sum_\Lambda y^\Lambda_{\mu_0}(\theta)\frac{e^{i\Lambda\zeta}}{\sqrt{2\pi}}. \quad \text{(A13)}$$

The initial rovibrational target state $\chi_{\nu_i}(Q)$ is expanded in a basis of Wigner rotation matrices as per Eq. (58). With the

axial recoil approximation of Eq. (A11), the solution of the LCP equation ξ_{ν_i} can then be written

$$\xi_{\nu_i}(\vec{Q}) = \sum_{\Lambda} y^{\Lambda}_{\mu_0}(\theta) \sum_{K} \tilde{D}^{J}_{M(K-\Lambda)}(\phi,\theta,\zeta) \frac{e^{i\Lambda\zeta}}{\sqrt{2\pi}} \times \int d\vec{q}'_{\rm int} g^{+}_{J_r K}(\vec{q}_{\rm int};\vec{q}'_{\rm int};E) V_{\mu_0}(\vec{q}'_{\rm int}) \chi^{(K-\Lambda)}_{\nu_i}(\vec{q}'_{\rm int}). \tag{A14}$$

For a triatomic, the final state of the system is

$$\psi^{\nu}_{B} = \chi_{\nu}(r) Y_{jK}(\gamma,\zeta) = \chi_{\nu}(r) \tilde{P}_{jK}(\gamma) \frac{e^{iK\zeta}}{\sqrt{2\pi}}, \tag{A15}$$

where χ_ν and Y_{jK} are, respectively, the vibrational and rotational wave functions of the diatomic fragment, and $\tilde{P}_{jK}$ is a normalized associated Legendre function. We omit the j dependence of the vibrational states. Therefore, the differential cross section for producing a final state with quantum numbers ν, j, K is

$$\frac{\partial \sigma^{\nu jK}_{\rm DEA}}{\partial \Omega_k} = \lim_{R\to\infty} \frac{2\kappa_{\tau\upsilon}}{\mu_R k^2} R^2 \sum_{\Lambda\Lambda'} (\chi_\nu \tilde{P}_{jK} | \hat{g}^{+}_{KJ_r} | V_{\mu_0} \chi^{K-\Lambda}_{\nu_i}) \times (\chi_\nu \tilde{P}_{jK} | \hat{g}^{+}_{J_r} | V_{\mu_0} \chi^{K-\Lambda'}_{\nu_i})^{*} \times y^{\Lambda}_{\mu_0}(\theta) y^{\Lambda' *}_{\mu_0}(\theta) \tilde{d}^{J}_{MK-\Lambda}(\theta) \tilde{d}^{J}_{MK-\Lambda'}(\theta). \tag{A16}$$

To obtain the physically observable cross section, we average over M and sum over K quantum numbers. We also make use of the orthonormality relation

$$\frac{2}{2J+1} \sum_{M} \tilde{d}^{J}_{M\Lambda}(\theta) \tilde{d}^{J}_{M\Lambda'}(\theta) = \delta_{\Lambda,\Lambda'} \tag{A17}$$

to obtain the result

$$\frac{1}{2J+1} \sum_{MK} \frac{\partial \sigma^{\nu jK}_{\rm DEA}}{\partial \Omega_k} = \lim_{R\to\infty} \frac{\kappa_{\tau\upsilon}}{\mu_R k^2} R^2 \sum_{\Lambda} |y^{\Lambda}_{\mu_0}(\theta)|^2 \times \sum_{K} |(\chi_\nu P_{jK} | \hat{g}^{+}_{J_r K} | V_{\mu_0} \chi^{K-\Lambda}_{\nu_i})|^2. \tag{A18}$$

Since individual rotational levels are generally not resolved in contemporary experiments, the measured cross sections average over an emsemble of initial and final states populated in the experiment. We therefore argue that the sum over K in Eq. (A18) may be taken to be independent of Λ once an average over the initial and final rotational states populated in the experiment is performed, i.e., that the rotational excitation of the initial state does not affect the amplitudes for producing final vibrational states in any coherent way. It then follows that the angular dependence of the observable differential cross section factors as

$$\frac{\partial \sigma^{\nu}_{\rm DEA\ exp't}}{\partial \Omega_k} \approx \sigma^{\nu}_{\rm DEA} \sum_{\Lambda} |y^{\Lambda}_{\mu_0}(\theta)|^2 = \sigma^{\nu}_{\rm DEA} \int d\zeta |y_{\mu_0}(\theta,\zeta)|^2. \tag{A19}$$

The result that the angular dependence of the cross section should be independent of the product state vibrational quantum number depends on the constant-eigenmode factorization $V_{\mu_0}(\vec{q}_{\rm int}) \times y_{\mu_0}(\theta,\zeta)$ of the entrance amplitude. In cases where this constant-eigenmode approximation does not hold, as we found for H_2S, we may still expand $V_{\bar{a}}$ as

$$V_{\bar{a}} = \sum_{\Lambda} V_{\Lambda}(\vec{q}_{\rm int},\theta) \frac{e^{i\Lambda\zeta}}{\sqrt{2\pi}}, \tag{A20}$$

in which case we arrive at the expression

$$\frac{1}{2J+1} \sum_{MK} \frac{\partial \sigma^{\nu jK}_{\rm DEA}}{\partial \Omega_k} = \lim_{R\to\infty} \frac{\kappa_{\tau\upsilon}}{2\mu_R k^2} R^2 \times \sum_{\Lambda K} |(\chi_\nu P_{jK} | \hat{g}^{+}_{J_r K} | V_{\Lambda}(\theta) \chi^{K-\Lambda}_{\nu_i})|^2. \tag{A21}$$

Thus, the angular dependence of the cross sections for different final vibrational states then requires explicitly solving the nuclear local complex potential equation for different values of θ in the entrance amplitude. For our calculations on H_2S, we evaluated this expression using an initial state wave function, and a Hamiltonian for the propagation, with $J=0$, $K=0$.

[1] D. J. Haxton, Z. Zhang, C. W. McCurdy, and T. N. Rescigno, Phys. Rev. A **69**, 062713 (2003).
[2] D. J. Haxton, Z. Zhang, H.-D. Meyer, T. N. Rescigno, and C. W. McCurdy, Phys. Rev. A **69**, 062714 (2003).
[3] W. N. Lozier, Phys. Rev. **36**, 1417 (1930).
[4] I. S. Buchel'nikova, Zh. Eksp. Teor. Fiz. **35**, 1119 (1959).
[5] G. J. Schultz, J. Chem. Phys. **44**, 3856 (1966).
[6] R. N. Compton and L. G. Christophorou, Phys. Rev. **154**, 110 (1967).
[7] C. E. Melton, J. Chem. Phys. **57**, 4218 (1972).
[8] L. Sanche and G. J. Schultz, J. Chem. Phys. **58**, 479 (1972).
[9] S. Trajmar and R. I. Hall, J. Phys. B **7**, L458 (1974).
[10] D. S. Belić, M. Landau, and R. I. Hall, J. Phys. B **14**, 175 (1981).
[11] M. G. Curtis and I. C. Walker, J. Chem. Soc., Faraday Trans. **88**, 2805 (1992).
[12] C. R. Claydon, G. A. Segal, and H. S. Taylor, J. Chem. Phys. **54**, 3799 (1971).

[13] M. Jungen, J. Vogt, and V. Staemmler, Chem. Phys. **37**, 49 (1979).
[14] T. J. Gil, T. N. Rescigno, C. W. McCurdy, and B. H. Lengsfield, Phys. Rev. A **49**, 2642 (1994).
[15] L. A. Morgan, J. Phys. B **31**, 5003 (1998).
[16] J. D. Gorfinkel, L. A. Morgan, and J. Tennyson, J. Phys. B **35**, 543 (2002).
[17] R. Azria, Y. L. Coat, G. Lefevre, and D. Simon, J. Phys. B **12**, 679 (1979).
[18] T. N. Rescigno, C. W. McCurdy, A. E. Orel, and B. H. Lengsfield III, in *Computational Methods for Electron-Molecule Collisions*, edited by W. M. Huo and F. A. Gianturco (Plenum, New York, 1995).
[19] T. N. Rescigno, B. H. Lengsfield III, and C. W. McCurdy, in *Modern Electronic Structure Theory*, edited by D. R. Yarkony (World Scientific, Singapore, 1995), Vol. 1, pp. 501–588.
[20] H.-D. Meyer, U. Manthe, and L. S. Cederbaum, Chem. Phys. Lett. **165**, 73 (1990).
[21] U. Manthe, H.-D. Meyer, and L. S. Cederbaum, J. Chem. Phys. **97**, 3199 (1992).
[22] M. Beck, A. Jäckle, G. Worth, and H.-D. Meyer, Phys. Rep. **324**, 1 (2000).
[23] H.-D. Meyer and G. A. Worth, Theor. Chem. Acc. **109**, 251 (2003).
[24] T. F. O'Malley and H. S. Taylor, Phys. Rev. **176**, 207 (1968).
[25] D. T. Birtwistle and A. Herzenberg, J. Phys. B **4**, 53 (1971).
[26] L. Dube and A. Herzenberg, Phys. Rev. A **20**, 194 (1979).
[27] J. N. Bardsley and J. M. Wadehra, J. Chem. Phys. **78**, 7227 (1983).
[28] T. F. O'Malley, Phys. Rev. **150**, 14 (1966).
[29] W. Domke, Phys. Rep. **208**, 97 (1991).
[30] A. U. Hazi, A. E. Orel, and T. N. Rescigno, Phys. Rev. Lett. **46**, 918 (1981).
[31] A. U. Hazi, T. N. Rescigno, and M. Kurilla, Phys. Rev. A **23**, 1089 (1981).
[32] H. Feshbach, Ann. Phys. (N.Y.) **19**, 287 (1962).
[33] G. A. Worth, M. H. Beck, A. Jäckle, and H.-D. Meyer, The MCTDH Package, Version 8.2, (2000). See http://www.pci.uni-heidelberg.de/tc/usr/mctdh/
[34] J. Tennyson and B. T. Sutcliffe, J. Chem. Phys. **77**, 4061 (1982).
[35] J. R. Taylor, *Scattering Theory: The Quantum Theory of Nonrelativistic Collisions* (Wiley, New York, 1972).
[36] T. H. Dunning, J. Chem. Phys. **53**, 2823 (1970).
[37] W. J. Hunt and W. A. Goddard, Chem. Phys. Lett. **3**, 414 (1969).
[38] L. F. Pacios and P. A. Christiansen, J. Chem. Phys. **82**, 2664 (1985).
[39] A. Persky, J. Chem. Phys. **66**, 2932 (1977).
[40] J. Senekowitch, S. Carter, A. Zilch, H.-J. Werner, N. C. Handy, and P. Rosmus, J. Chem. Phys. **90**, 783 (1989).
[41] J. Z. H. Zhang, *Theory and Application of Quantum Molecular Dynamics* (World Scientific, Singapore, 1999).
[42] A. R. Edmonds, *Angular Momentum in Quantum Mechanics* (Princeton University Press, Princeton, NJ, 1996).
[43] C. Petrongolo, J. Chem. Phys. **89**, 1297 (1988).
[44] S. Sukiasyan and H.-D. Meyer, J. Phys. Chem. A **105**, 2604 (2001).
[45] R. G. Newton, *Scattering Theory of Particles and Waves*, 2nd ed. (Springer-Verlag, New York, 1982).
[46] T. Mulloney and G. C. Schatz, Chem. Phys. **45**, 213 (1980).
[47] R. T. Pack, Chem. Phys. Lett. **108**, 333 (1984).
[48] V. Khare, D. J. Kouri, and M. Baer, J. Chem. Phys. **71**, 1188 (1979).